

Article

Active Vibration Control Using Loudspeaker-Based Inertial Actuator with Integrated Piezoelectric Sensor

Minghao Chen, Qibo Mao , Lihua Peng and Qi Li

School of Aircraft Engineering, Nanchang HangKong University, 696 South Fenghe Avenue, Nanchang 330063, China; 2206082500003@stu.nchu.edu.cn (M.C.); penglihua2021@163.com (L.P.); 1921123187@163.com (Q.L.)

* Correspondence: qbmao@nchu.edu.cn; Tel.: +86-150-7913-1754

Abstract: With the evolution of the aerospace industry, structures have become larger and more complex. These structures exhibit significant characteristics such as extensive flexibility, low natural frequencies, numerous modes, and minimal structural damping. Without implementing vibration control measures, the risk of premature structural fatigue failure becomes imminent. In present times, the installation of inertial actuators and control signal acquisition units typically requires independent setups, which can be cumbersome for practical engineering purposes. To address this issue, this study introduces a novel approach: an independent control unit combining a loudspeaker-based inertial actuator (LBIA) with an integrated piezoelectric ceramic sensor. This unit enables autonomous vibration control, offering the advantages of ease of use, low cost, and lightweight construction. Experimental verification was performed to assess the mechanical properties of the LBIA. Additionally, a mathematical model for the LBIA with an integrated piezoelectric ceramic sensor was developed, and its efficacy as a control unit for thin plate structure vibration control was experimentally validated, showing close agreement with numerical results. Furthermore, the LBIA's benefits as an actuator for low-frequency mode control were verified through experiments using external sensors. To further enhance control effectiveness, a mathematical model of the strain differential feedback controller based on multi-bandpass filtering velocity improvement was established and validated through experiments on the clamp–clamp thin plate structure. The experimental results demonstrate that the designed LBIA effectively reduces vibration in low-frequency bands, achieving vibration energy suppression of up to 12.3 dB and 23.6 dB for the first and second modes, respectively. Moreover, the LBIA completely suppresses the vibration of the fourth mode. Additionally, the improved control algorithm, employing bandpass filtering, enhances the effectiveness of the LBIA-integrated sensor, enabling accurate multimodal damping control of the structure's vibrations for specified modes.

Keywords: active vibration control; loudspeaker-based inertial actuator; feedback control



Citation: Chen, M.; Mao, Q.; Peng, L.; Li, Q. Active Vibration Control Using Loudspeaker-Based Inertial Actuator with Integrated Piezoelectric Sensor. *Actuators* **2023**, *12*, 390. <https://doi.org/10.3390/act12100390>

Academic Editors: Ti Chen, Junjie Kang, Shidong Xu and Shuo Zhang

Received: 12 September 2023

Revised: 13 October 2023

Accepted: 13 October 2023

Published: 17 October 2023



Copyright: © 2023 by the authors. Licensee MDPI, Basel, Switzerland. This article is an open access article distributed under the terms and conditions of the Creative Commons Attribution (CC BY) license (<https://creativecommons.org/licenses/by/4.0/>).

1. Introduction

Vibration presents substantial challenges in aerospace engineering, as it embodies unwanted energy that can trigger aeroelastic instability, particularly flutter. Additionally, aircraft vibration can induce fatigue, generate excessive noise, and cause discomfort for passengers and crew. Consequently, it becomes imperative to implement efficient vibration control methods to ensure both structural integrity and overall vehicle safety. Among the various vibration control strategies, passive control usually uses dynamic vibration absorbers (DVAs), which are extensively employed for controlling structural vibrations [1–5]. However, one drawback of DVAs is their limited effectiveness in attenuating vibrations at multiple resonance frequencies. Significant advancements have been achieved by implementing inertial actuators (or proof mass actuators) [6,7], resulting in improved reduction of vibrations across multiple resonance frequencies [8]. These actuators exhibit enhanced adaptability to changes in controlled structural parameters, making them suitable for

a wide range of operating conditions including low-frequency scenarios where precise vibration control is required. Over the past two decades, inertial actuators have found extensive use as vibration and structural sound suppression devices, demonstrating their high effectiveness in reducing vibrations during bridge construction [9] and minimizing noise levels in aircraft cabins, thereby enhancing safety and passenger comfort [10,11].

To date, many active vibration control (AVC) strategies have utilized a centralized architecture based on negative velocity feedback, which allows for precise damping of structural vibrations [12–15]. However, as the control system expands, potential issues may arise, particularly in cases of sensor failure, which can result in a complete system breakdown. In contrast, a totally decentralized control strategy allows each control unit to operate independently, also known as self-sufficient controllers [16,17]. In this strategy, inertial actuators and accelerometers are employed, with their signals processed by a time integrator to serve as control units in active control systems, enabling precise control over structural vibrations. To ensure system stability, it is crucial to align the sensors and actuators perfectly during application. However, this method often presents imperfect alignment control during installation [18]. If the inertial actuator and sensor are designed as a monolithic structure, perfect alignment of the system can be ensured and the stability of the system is theoretically guaranteed [19].

On the other hand, the distributed control strategy in vibration control systems often necessitates complex alignment of each control unit [20,21]. A massive number of sensors and actuators need to be installed and the operation is very complex [22]. Meanwhile, commercially available velocity sensors currently suffer from drawbacks such as their large size, high cost, and inconvenient usage [23]. Additionally, displacement sensors or acceleration sensors require corresponding circuitry to convert their outputs into velocity signals. To overcome the drawback of complex alignment, a novel solution has been developed: a self-sufficient control unit [17]. This innovative device enables precise alignment control and integrates a compact, portable velocity sensor directly into the control unit, eliminating the need for external circuit modules. It combines the basic elements of a control unit, containing a velocity sensor for vibration detection and an actuator driven by a control signal.

Apart from the design of the inertial actuators, selecting an appropriate active control algorithm is crucial to improve control efficiency. One rather appealing solution for the active control of broadband vibration is using self-contained control units with direct velocity feedback (DVBF) laws implemented through velocity sensors and collocated inertial actuator pairs. These control units are achieved by employing a velocity sensor or an accelerometer processed by an external integrated circuit and a parallel inertial actuator pair, eliminating the need for an external support to react off; thus, the control unit is simple to mount on the structure to be controlled [24].

Earlier work focused on implementing a decentralized array of DVBF control units with the ability to adjust the feedback gain to reduce the structure's vibration significantly [25]. Additionally, Zilletti et al. [26] demonstrated that maximizing power absorption is equivalent to minimizing the kinetic energy if the primary structure is an SDOF structure. By increasing the feedback gain, the peak resonance frequency of the SDOF system decreases due to the active damping effect. However, the dynamic behavior of the inertial actuator leads to overflow at its resonant frequency, making the system unstable as the feedback gain approaches the maximum steady-state gain. To solve this problem, the optimal feedback gain of the vibration control board can be achieved by maximizing the power absorption [27,28]. Moreover, the margin of feedback gain can be further improved by phase compensation of inertial actuators or other control algorithms, thus enhancing the stability of the system.

Among these control algorithms, positive position feedback (PPF) stands out as a second-order low-pass filter widely used in structural vibration control due to its simplicity, robustness, and effectiveness in addressing high-frequency signal saturation [29–32]. Notably, Fanson and Caughey first proposed the PPF control technique; PPF is insensitive to the uncertainty of the structure's natural damping ratio, providing stable and reliable

vibration control [33–35]. The term “positive position” refers to feeding position measurements into the compensator in a positive manner and positively feeding position signals from the compensator back to the structure [3]. This characteristic makes this algorithm well-suited for collocated actuator/sensor pairs [36–38]. Previous research by Friswell and Inman proposed PPF control as an output feedback controller, using optimal control technology to address the instability problem caused by not considering mode overflow in the SDOF system. The effectiveness of this method was verified using centralized and distributed control architectures [39]. Similarly, Sim and Lee used an accelerated feedback (AFC) strategy employing second-order filters, also known as resonant controllers, to target desired modes of multi-degree-of-freedom systems [40,41]. Zhao et al. studied the application of a nonlinear positive position feedback controller with Duffing oscillator and derived the closed expression of optimal control parameters [42]. As a result, the low-pass filter as a PPF controller has been shown to work well for signal or multimodal control [43].

However, using multiple low-pass filters as PPF controllers to control multimodal vibrations may lead to phase overlap and potential multimodal control problems. The combined action of multiple PPF controllers affects the overall phase response of the system, making it challenging to control multiple modes simultaneously. Furthermore, incorrect placement of the second PPF controller may interfere with the operation of the first one, rendering it ineffective [44]. To enhance the control stability of the inertial actuator under the DVBF method, this study adopts a bandpass filter based on the second-order compensator principle proposed by Rohlfing [14]. The objective is to address the problem and improve the traditional DVBF stability. By adjusting the center frequency and damping of each bandpass filter, precise control of different modes can be achieved; then, overall system stability can be improved. This method offers a promising solution for improving phase-related issues and enhancing the effectiveness of multimodal control in vibration reduction.

The rest of this study is structured as follows. In Section 2, the designed loudspeaker-based inertial actuator with an integrated piezoelectric sensor will be described and experimentally verified. Section 3 presents the control performances of the proposed LBIA by using the DVBF approach for thin plate structures. In addition, the piezoelectric sensor model of the integrated control unit is established. In Section 4, a parallel connection of multiple bandpass filters is used as a controller to improve the control performance based on the proposed LBIA; then, the corresponding experimental results are presented. Section 5 concludes with a discussion and summary of the relevant research results and experimental conclusions.

2. LBIA with Integrated Piezoelectric Sensor Configuration and Performance

2.1. LBIA with Integrated Piezoelectric Sensor Design

The inertial actuator consists of several essential components, such as an electromagnetic coil, permanent magnet, elastic element, and base. Its operation relies on supplying power to the electromagnetic induction coil, which induces specific and regular changes in the surrounding magnetic field. As a result, the Lorentz force is generated, propelling the reciprocal motion of the actuator and permanent magnet. With these fundamental principles and components in mind, it becomes apparent that the loudspeaker principle seamlessly aligns with the inertial actuator. Therefore, it is possible to modify a loudspeaker as an inertial actuator, as depicted in Figure 1.

The loudspeaker employed in this design is a moving-coil loudspeaker, commonly referred to as an electric loudspeaker. Upon inputting the control signal to the loudspeaker, the resulting Lorentz force propels the paper cone to reciprocate, thereby generating the desired control force. To optimize the effectiveness of the control force, the surface of the paper cone is connected to a natural rubber base using neutral silicone rubber. This rubber support base enhances the overall actuator performance and improves passive control effects. Neutral silicone rubber possesses favorable characteristics such as lower damping,

reduced energy absorption, and efficient transfer of the control force, making it an ideal material choice for the base.

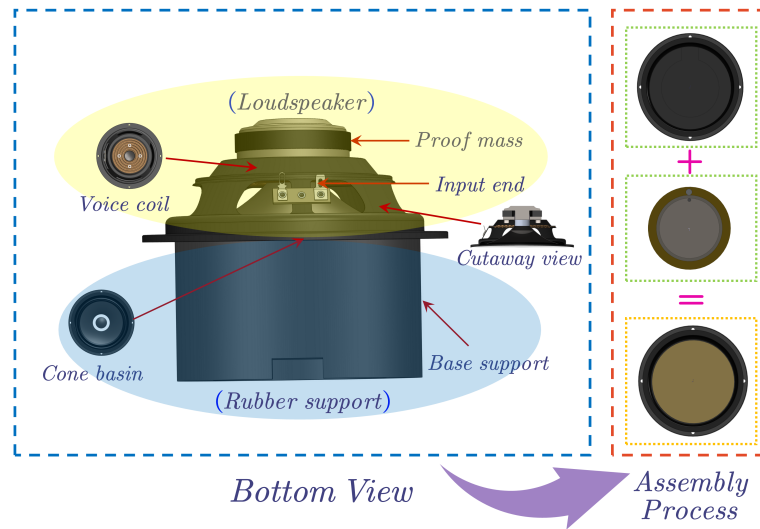


Figure 1. Configuration design of loudspeaker-sensor integrated actuator.

Furthermore, it is essential to highlight that Figure 1 illustrates the utilization of a thin-film piezoelectric ceramic sensor with a small volume and electrodes positioned on its surface. To ensure accurate measurement and prevent contact with the sensor’s electrode surface, a ring-shaped support base is employed, facilitating the integrated design of the sensor and actuator. This configuration allows the applied force to be transmitted to the vibrating structure’s surface through the ring shape, approximating the force as a point force based on findings from [40]. This feature makes it well-suited for active vibration control.

A photograph of the proposed LBIA is presented in Figure 2. The mechanical and electrical parameters of the LBIA are listed in Table 1. Notice that the proposed LBIA also integrates a piezoelectric sensor, resulting in an integrated control unit. This integration greatly improves installation efficiency and reduces the occurrence of poor stability due to alignment errors.

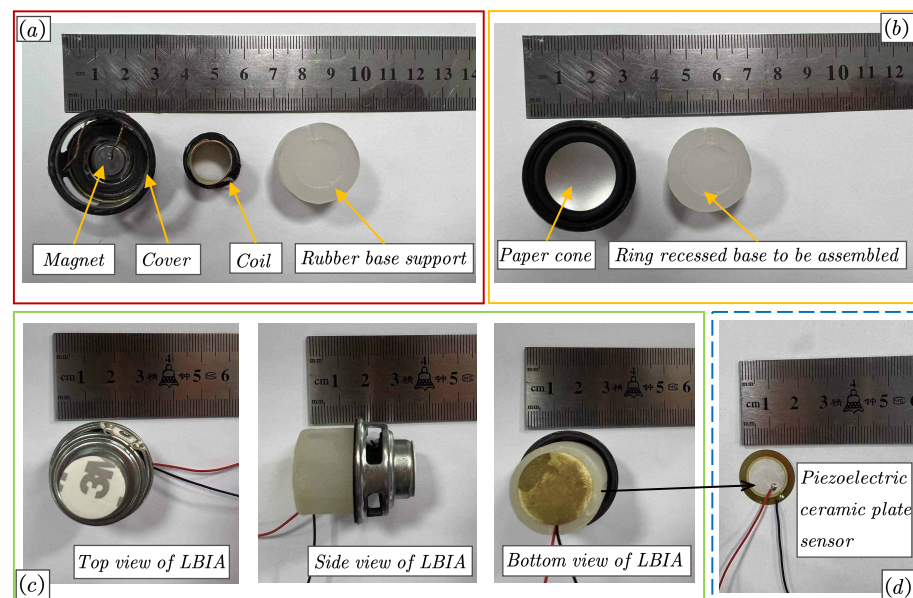


Figure 2. LBIA with integrated piezoelectric sensor: (a) before assembly; (b) partial assembly; (c) after assembly; (d) sensor.

Table 1. Performance of the inertial actuator (LBIA).

Parameter	Notation	Value	Unit
Proof mass	M_a	0.0236	kg
Base support mass	M_b	0.0088	kg
Suspension stiffness	K_a	2800	N/m
Suspension damping coefficient	C_a	0.2	Ns/m
Natural frequency	ω_n	55	Hz
Damping ratio	ζ	5.2252	
Voice coil coefficient	Bl	0.018	N/A
Coil resistance	R_e	4	Ω
Coil inductance	L_e	88.1×10^{-5}	H

2.2. Dynamic Model for LBIA

This subsection focuses on describing the dynamic characteristics of the LBIA itself. Since the loudspeaker is an electromechanical coupling system, a corresponding dynamic model can be established based on this, and the specific schematic diagram is shown in Figure 3.

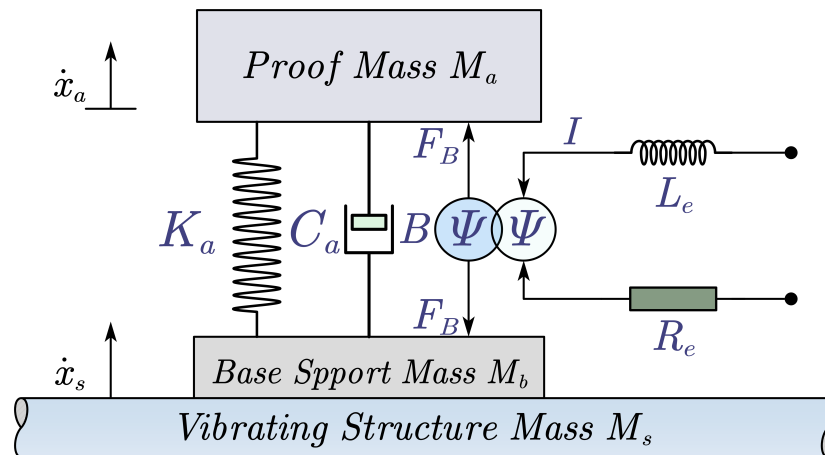


Figure 3. The electromechanical schematic for LBIA with integrated piezoelectric sensor.

The loudspeaker itself outputs volume velocity, which excites the mass block of the supporting base. Additionally, considering the mechanical characteristics of the actuator on the main structure, a coupling dynamic model between the inertial actuator and the main structure is established. This model can be considered a mass-spring-damping system, as shown in Figure 3. The dynamic model can be expressed as follows:

$$M_a \ddot{x}_a + C_a(\dot{x}_a - \dot{x}_s) + K_a(x_a - x_s) = Bl \cdot I = F_B \tag{1}$$

$$U_{in} = B(\dot{x}_a - \dot{x}_s) + R_e I + L_e \dot{I} \tag{2}$$

where U_{in} is the input voltage of the inertial actuator, and x_a and x_s are the displacement of the proof mass and base support of the inertial actuator, respectively.

The controlling force (inertial force) output of the inertial actuator is

$$F_c = Bl \cdot I - C_a \dot{x}_a - K_a x_a \tag{3}$$

In the state-space domain way, the actuator dynamics from Equations (1)–(3) can be rearranged as

$$\begin{cases} \dot{\mathbf{x}} = \mathbf{A}\mathbf{x} + \mathbf{B}U_{in} \\ F_c = \mathbf{C}\mathbf{x} + \mathbf{D}U_{in} \end{cases} \tag{4}$$

where the output F_c is the control force vector generated by the actuators. In the voltage-driven configuration, the state of the system is completely defined by both differential

equations in Equations (1) and (2). Therefore, the state vector includes the current as $\mathbf{x}^T = [x \quad \dot{x} \quad I]$.

The state matrices are, respectively,

$$\mathbf{A} = \begin{bmatrix} 0 & 1 & 0 \\ -\frac{K_a}{M_a} & -\frac{C_a}{M_a} & \frac{B}{M_a} \\ 0 & -\frac{B}{L_e} & \frac{R_e}{L_e} \end{bmatrix}, \quad \mathbf{B} = \begin{bmatrix} 0 \\ 0 \\ \frac{1}{L_e} \end{bmatrix}, \quad \mathbf{C} = \begin{bmatrix} -K_a \\ -C_a \\ B \end{bmatrix}^T, \quad \mathbf{D} = 0 \quad (5)$$

According to the state space method, the transfer function of the input voltage to the output force of the inertial actuator can be obtained as follows:

$$T_a(\omega) = \frac{F_c(\omega)}{U_{in}(\omega)} = \mathbf{C}(j\omega\mathbf{E} - \mathbf{A})^{-1}\mathbf{B} \quad (6)$$

Equation (6) reflects the relationship between the input signal and the output force of the actuator. Based on Equation (6), the mechanical characteristics of the actuator can be solved, which provides a reference for the selection of the active control algorithm.

2.3. LBIA Performance Test

To obtain the mechanical performance of the proposed LBIA, the actuator’s output characteristics were tested to study the variation in output force and the effective working frequency range. Based on this, a test platform was constructed, as depicted in Figure 4.

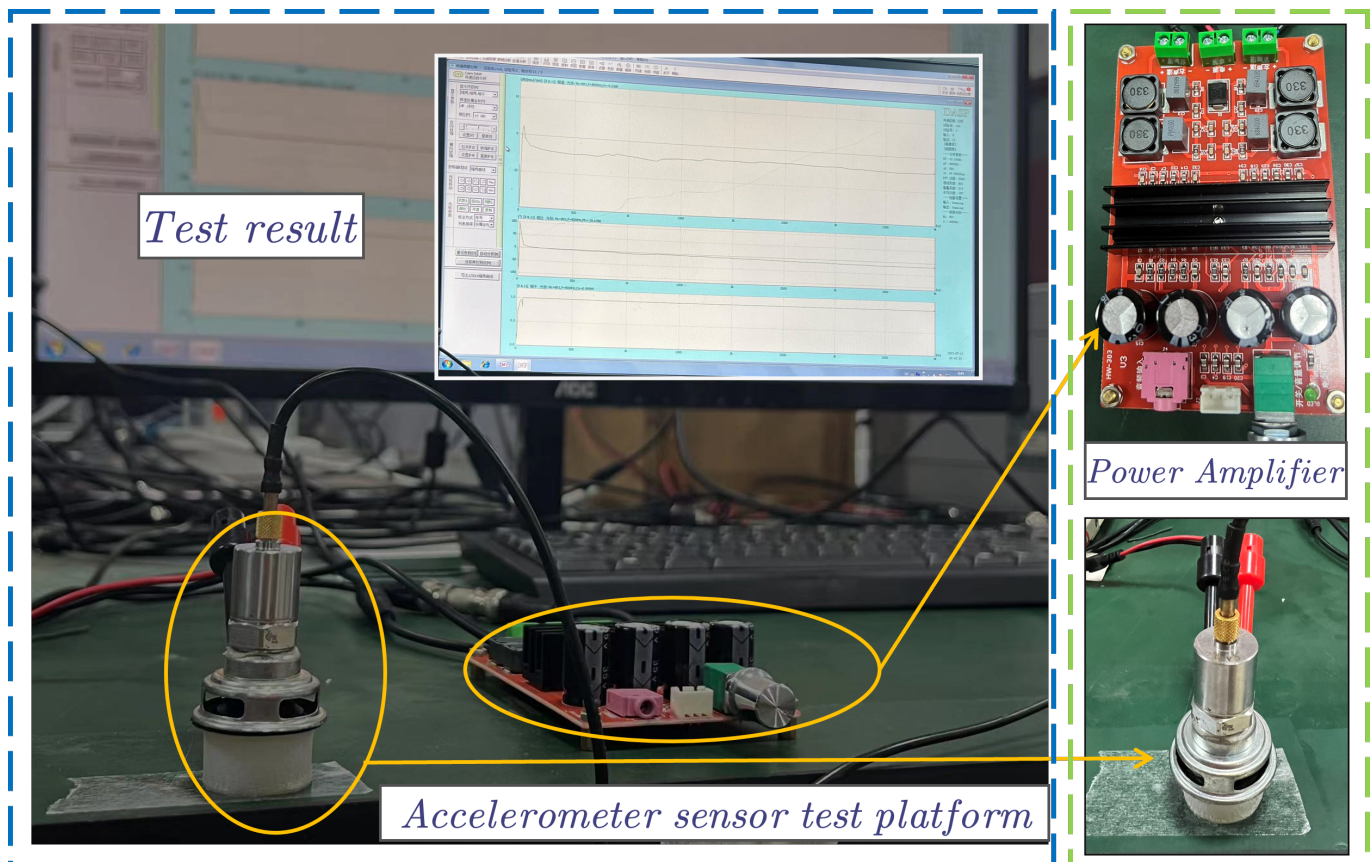


Figure 4. Picture of the experimental setup for measuring mechanical performance of LBIA with integrated piezoelectric sensor.

Figure 4 shows the experimental setup for measuring the mechanical performance of the inertial actuator. The experimental measurements focused on establishing the relationship between the amplitude of the LBIA with the integrated piezoelectric sensor input signal and the input force. To evaluate the mechanical performance, a YD-186 accelerometer from Sinocera Piezotronics Inc. (Yangzhou, China) (with a weight of 30 g and sensitivity of $10.2 \text{ mv}/(\text{ms}^{-2})$) was installed on the proof mass and base support of the LBIA with an integrated piezoelectric sensor to measure its acceleration. The COINV dynamic signal analyzer (Beijing, China) (which has 24 channels but only uses the first two channels) was used to obtain its frequency response function. The mechanical properties of the inertial actuator can then be determined.

Importantly, the negligible mass (approximately 0.1 g) of the piezoelectric ceramic sensor allows us to disregard it; thus, it was not installed during the tests, as shown in Figure 4. However, the mass of the accelerometer cannot be disregarded for the LBIA. The output characteristics can be expressed as

$$T_a = \frac{F_c}{U_{in}} = \frac{M_a a_a}{U_{in}} \text{ s.t. } v_s = 0 \tag{7}$$

During the variable amplitude output force response test, a range of sinusoidal signals with frequencies of 155 Hz and varying amplitudes were employed. The selected test signal had an input voltage from 50 mV to 350 mV, with test points recorded at 50 mV intervals. By utilizing Newton’s second law, the acceleration signals accurately portrayed the mechanical performance of the actuator. The experimental results are presented in Figure 5.

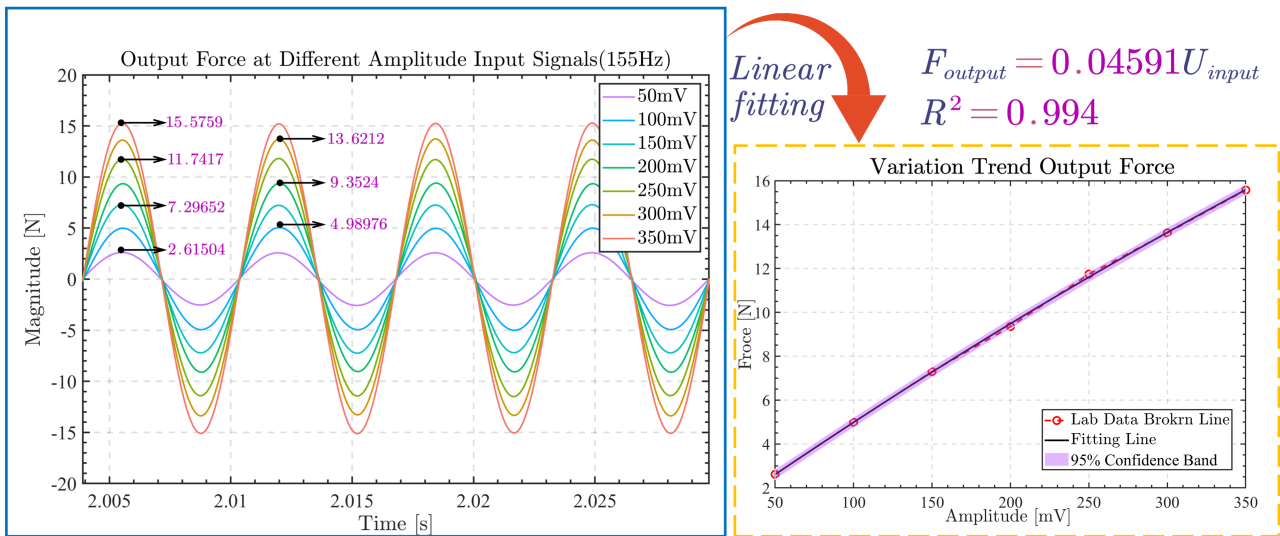


Figure 5. Output force test results at different input amplitude signals.

The test results show that at 155 Hz, the output force of the inertial actuator is accurate and free from distortion, aligning with the first mode of the controlled structure shown in Figure 5. Additionally, the output force of the inertial actuator shows a proportional increase in relation to the input amplitude, illustrating an approximate linear relationship with a goodness of fit value of 0.94.

For the variable frequency output force response test, a sinusoidal signal ranging from 10 Hz to 1000 Hz with an amplitude of 100 mV was utilized. Figure 6 illustrates that the natural frequency of LBIA is 30 Hz due to the accelerometer mass. Notably, the inertial actuator’s output control force remains relatively stable in both magnitude and phase when the frequency exceeds the natural frequency. In this frequency band, the inertial actuator effectively functions as an exciter, producing an ideal point force output. Additionally, the frequency response test results of the actuator align closely with the transfer function of the

theoretical model. The bearing shape and output force characteristics were also verified in [45].

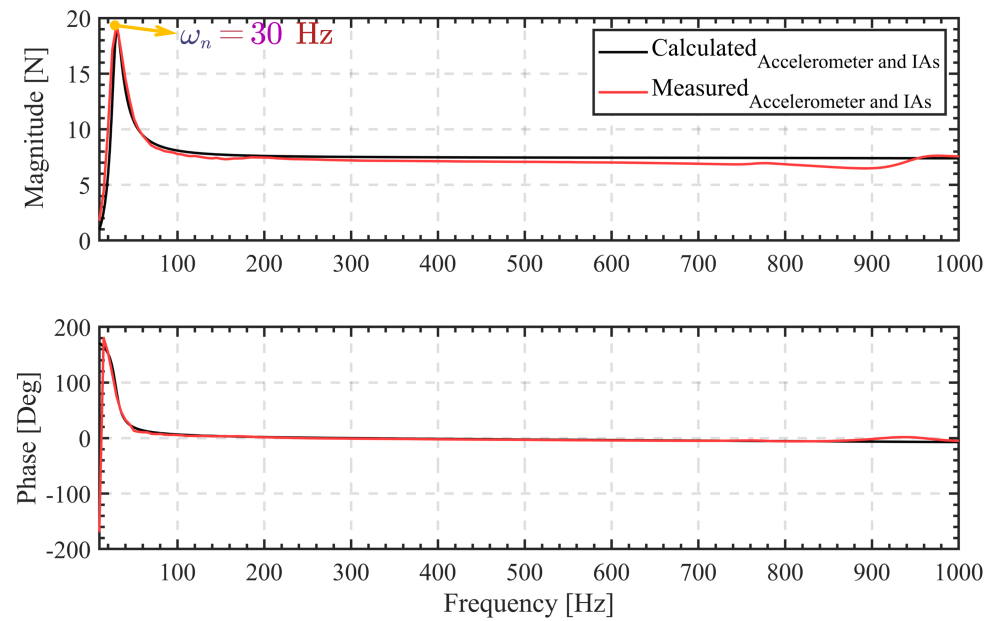


Figure 6. Output force test results at different frequencies.

From Figures 5 and 6, it can be found that the proposed LBIA offers several advantages:

- The whole configuration adopts an integrated design that is easy to disassemble, and because of the alignment design, the control system is stable;
- The speaker, serving as the actuator, produces sound vibrations characterized by low distortion and high fidelity. Its flat frequency response enables clear resolution and accurate reproduction of audio signals across a wide frequency range, from low to high;
- The rubber structure is used as the support structure, the structural damping is small, and the output control force can be effective.

This section demonstrates the establishment of an accurate dynamic model for the LBIA, offering valuable insights into its mechanical performance. Moreover, it serves as a foundational basis for further research on control algorithms.

3. Control Performance of LBIA with Integrated Piezoelectric Sensor by Using Strain Differential Feedback (SDF) Approach

In this section, our focus is to discuss the effectiveness of the integrated design as a control unit for thin plate structures. To demonstrate this, we utilize the strain differential feedback (SDF) approach based on the integrated piezoelectric ceramic sensor.

Figure 7 illustrates the behavior of the piezoelectric ceramic sensor under the influence of a stress field. When the sensor senses structural vibrations, it generates the corresponding induced electricity. According to [46], the induced charge generated by piezoelectric ceramic sensors can be described by Equation (8) as follows:

$$Q_e = \frac{h}{2} e \int_0^{2\pi} \int_0^R \left(\frac{\partial^2 w(r, \theta, t)}{\partial r^2} + \frac{1}{r} \frac{\partial w(r, \theta, t)}{\partial r} + \frac{1}{r^2} \frac{\partial^2 w(r, \theta, t)}{\partial \theta^2} \right) r dr d\theta \quad (8)$$

$$\text{for } \begin{cases} r = \sqrt{(x - x_0)^2 + (y - y_0)^2} \\ \theta = \text{atan2}(y - y_0, x - x_0) \end{cases}$$

where $w(r, \theta, t)$ is the polar coordinate form of displacement of the thin plate, e is the piezoelectric strain constant of the sensor, R is the radius of the selected circular piezoelectric

ceramic sensor, and x_0 and y_0 represent the central position of the piezoelectric ceramic sensor.

As depicted in Figure 7, the sensor generates a charge signal in response. This signal can be perceived as a voltage source connected in series with the capacitor. Once connected to a signal conditioning circuit—specifically, a current amplifier—the output signal undergoes conversion into a current signal. Reference [47] provides insights into the understanding of this process from both physical and mathematical perspectives, assuming the piezoelectric strain constant and alignment with the Y-axis. Essentially, it involves differentiating Equation (8) once. The current output of piezoelectric ceramics is expressed as follows:

$$I_e = \frac{dQ_e}{dt} = \frac{h}{2} e \int_0^{2\pi} \int_0^R \left(\frac{\partial^2 v(r, \theta)}{\partial r^2} + \frac{1}{r} \frac{\partial v(r, \theta)}{\partial r} + \frac{1}{r^2} \frac{\partial^2 v(r, \theta)}{\partial \theta^2} \right) r dr d\theta \quad (9)$$

Equation (9) can be expressed as

$$\begin{cases} v(r, \theta) = \sum_{k=1}^m \phi_k \Phi_k(r, \theta) = \Phi^T \phi \\ I_e = \frac{h}{2} e \int_0^{2\pi} \int_0^R \left(\sum_{k=1}^m \phi_k \frac{\partial^2 \Phi_k(r, \theta)}{\partial r^2} + \sum_{k=1}^m \frac{1}{r} \phi_k \frac{\partial \Phi_k(r, \theta)}{\partial r} + \sum_{k=1}^m \frac{1}{r^2} \phi_k \frac{\partial^2 \Phi_k(r, \theta)}{\partial \theta^2} \right) r dr d\theta \end{cases} \quad (10)$$

where $\Phi_k(r, \theta)$ and ϕ_k represent the m th structural modal shape and modal velocity, respectively. The modal index of the structure on the x and y axes is represented by $k = (m_x, m_y)$, respectively.

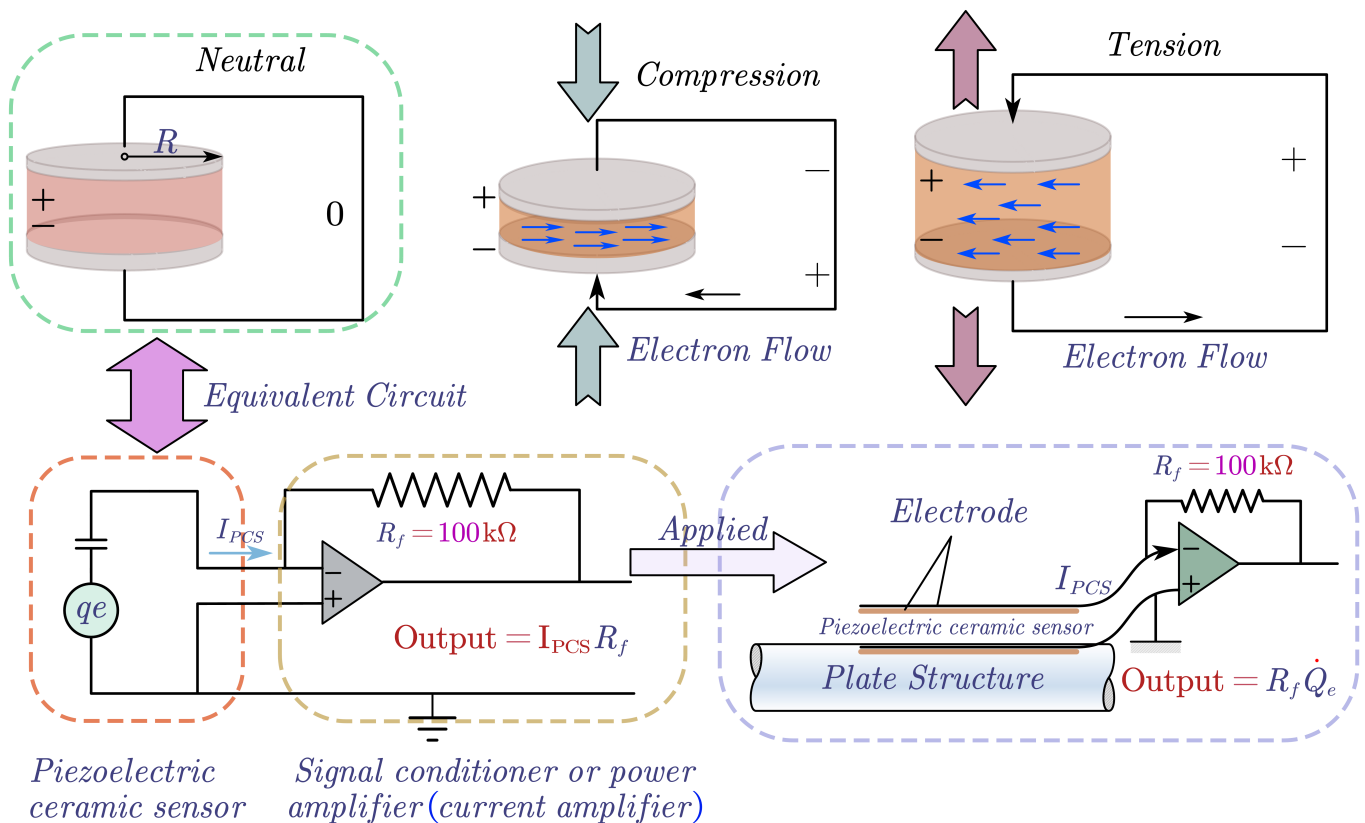


Figure 7. Schematic diagram of piezoelectric ceramic sensor.

Equation (10) can be further simplified to matrix form:

$$I_e = \mathbf{P}\boldsymbol{\phi} \quad (11)$$

$$P_k = \frac{h}{2} e \int_0^{2\pi} \int_0^R \left(\sum_{k=1}^m \frac{\partial^2 \Phi_k(r, \theta)}{\partial r^2} + \sum_{k=1}^m \frac{1}{r} \frac{\partial \Phi_k(r, \theta)}{\partial r} + \sum_{k=1}^m \frac{1}{r^2} \frac{\partial^2 \Phi_k(r, \theta)}{\partial \theta^2} \right) r dr d\theta \quad (12)$$

The output voltage of the sensor is determined under the assumption that the current amplifier operates ideally with infinite internal resistance:

$$U_{in} = R_f \dot{Q}_e = R_f I_e = R_f \mathbf{P}\boldsymbol{\phi} \quad (13)$$

where R_f is the amplifier constant.

The combination model of the piezoelectric ceramic sensor and the inertial actuator can be obtained by utilizing the mathematical model of the piezoelectric ceramic sensor and the dynamic model of the inertial actuator:

$$\begin{aligned} & \left[M_a (j\omega R_e - \omega^2 L_e) + C_a (j\omega L_e + R_e) + K_a \left(L_e + \frac{R_e}{j\omega} \right) + (Bl)^2 \right] \cdot \dot{x}_a \\ & = U_{in} \cdot \frac{\left(Bl (R_f \Gamma + Bl) + C_a (j\omega L_e + R_e) + K_a \left(L_e + \frac{R_e}{j\omega} \right) \right)}{R_f \Gamma} \end{aligned} \quad (14)$$

where Γ is a direct multiple relationship between the current I and the velocity \dot{x}_s , which is expressed as $\Gamma = \mathbf{P}\boldsymbol{\phi} / \dot{x}_s$.

Finally, the control situation of the actuator and piezoelectric ceramic sensor is expressed as a transfer function:

$$T_{SDF}(\omega) = \frac{\dot{x}_a}{U_{in}} = \frac{\left(Bl (R_f \Gamma + Bl) + C_a (j\omega L_e + R_e) + K_a \left(L_e + \frac{R_e}{j\omega} \right) \right)}{R_f \Gamma \left[M_a (j\omega R_e - \omega^2 L_e) + C_a (j\omega L_e + R_e) + K_a \left(L_e + \frac{R_e}{j\omega} \right) + (Bl)^2 \right]} \quad (15)$$

Meanwhile, Figure 8b experimentally illustrates the Nyquist diagram of the open-loop transfer function testing before and after signal conditioning of the sensor in the LBIA. The diagram demonstrates the sensor's ability to convert its charge (displacement signal) into current (velocity signal) after signal conditioning. Notably, it can be seen from Figure 8a that effective vibration control is achieved when the phase detection indicates that the first and second modes are close to 0 degrees.

Additionally, the fourth mode also exhibits a discernible control effect, as observed in the phase analysis. Moreover, conditioning the signal is accompanied by a 90-degree phase change, resulting from the charge signal transforming into a current signal through the conditioning circuit. It can be described as a differential process, and its specific derivation process is given by Equation (9). Based on this process, the active vibration control based on it can be referred to as strain differential feedback (SDF) control. In conclusion, this analysis provides valuable support for subsequent experiments.

Figure 9 depicts the experimental setup, comprising a thin aluminum plate as the subject of investigation. The geometrical and physical properties of the plate are summarized in Table 2. To stimulate the structure, a sinusoidal scanning signal, generated by the commercial inertial actuator (DAEX58FP electrodynamic exciter, Nikon, Tokyo, Japan), is used for excitation in a frequency range of 10 Hz to 800 Hz. The vibration signal is collected by a piezoelectric ceramic sensor integrated with LBIA and then passed through the power amplifier to form a closed-loop control system. To ensure a more realistic case study, the primary excitation positions on the board were deliberately chosen to avoid the node lines associated with the previous modes of the structure. The selected position (x_p, y_p) for the primary source was set at (125 mm, 65 mm). By adopting this approach, the lower-order modes are excited, allowing us to observe the effect of active control on their vibration modes. Similarly, to avoid the node line position, an LBIA with an integrated piezoelectric ceramic sensor is installed at $(x_c, y_c) = (120 \text{ mm}, 160 \text{ mm})$.

The experiment described in this paper involved collecting vibration energy signals at the same location as LBIA. Specifically, the vibration energy point of the measuring point is on the opposite side of the same-positioned thin plate as LBIA. These signals were obtained using a high-precision laser vibrometer (Polytec IVS-500, Karlsruhe, Germany). In addition to this, an accelerometer sensor was included in Figure 9 to observe vibrations at different positions. This served as a backup measure in case of laser vibrometer failure, ensuring the test’s success when integrated with the LBIA design that incorporates piezoelectric sensors.

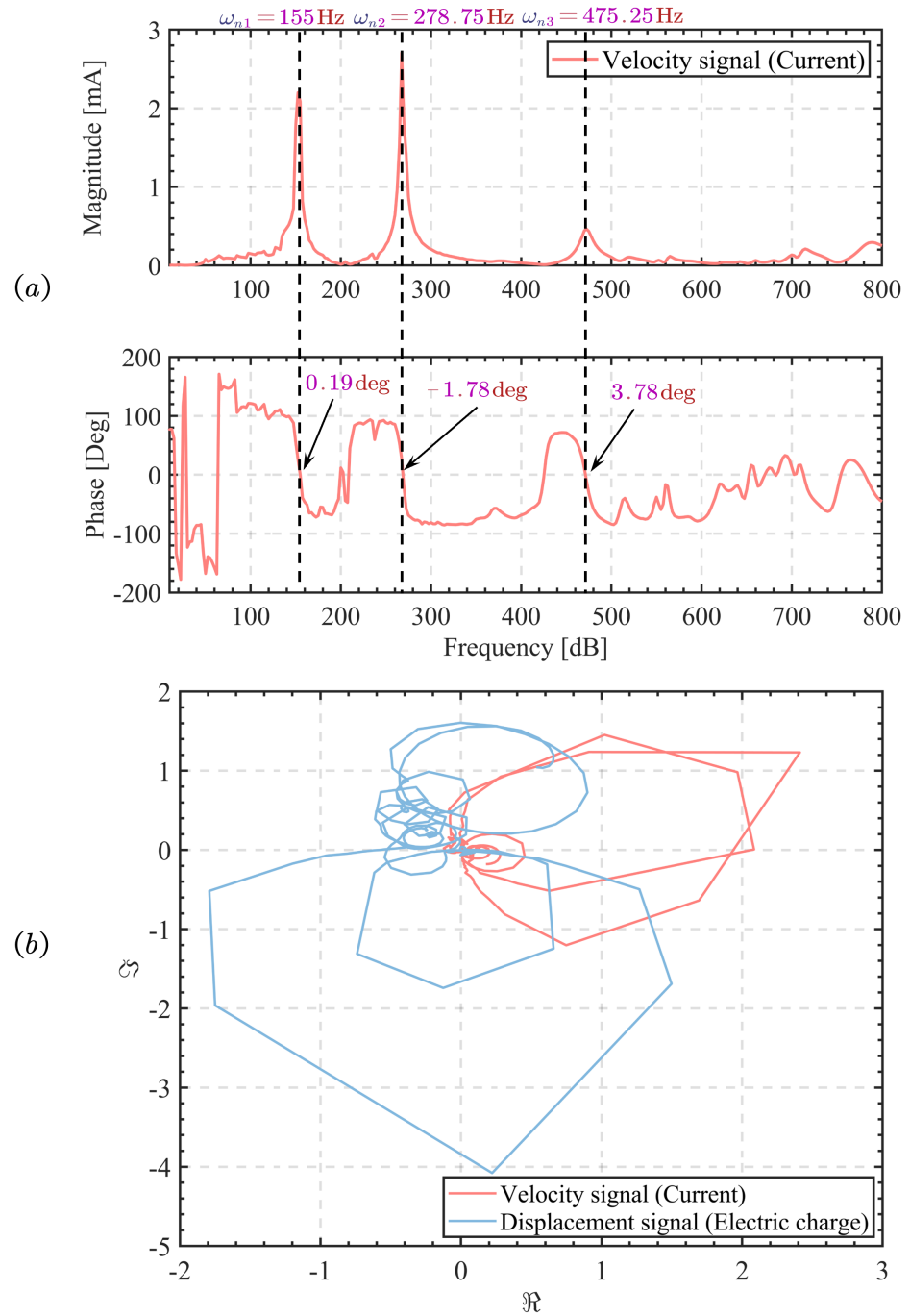


Figure 8. Open loop experiment diagram of integrated sensor in LBIA: (a) Bode diagram; (b) Nyquist diagram.

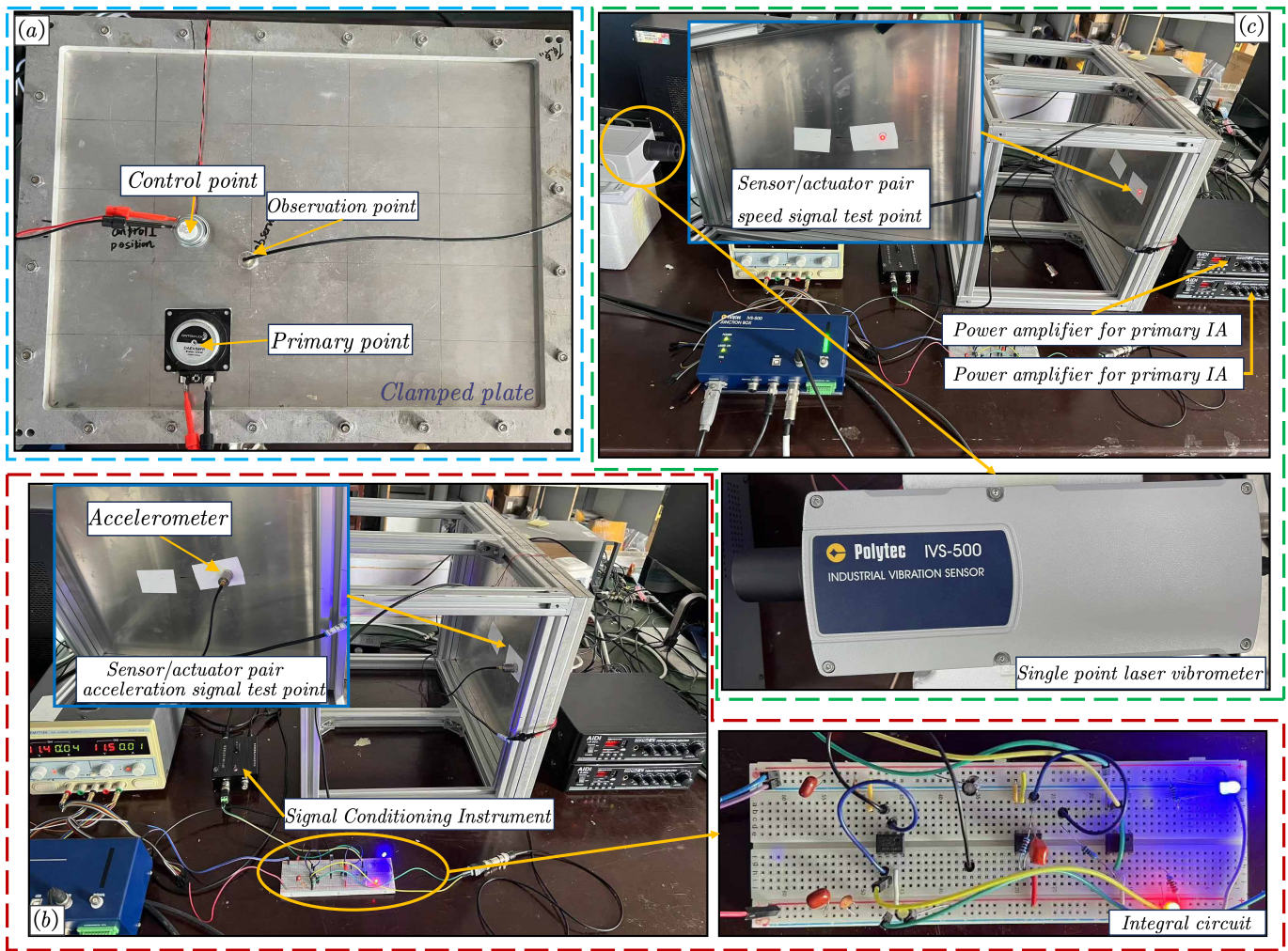


Figure 9. DVBF experiment of LBIA: (a) DVBF based on LBIA with integrated sensor; (b) DVBF based on accelerometer; (c) DVBF based on accelerometer.

Table 2. Geometry and physical parameters of the plate.

Parameter	Numerical Value	Unit
Planar dimensions	$l_x \times l_y = 440 \times 340$	mm
Thickness	$h = 3$	mm
Young’s modulus	$E = 7 \times 10^{10}$	N/m ²
Poisson ratio	$\nu = 0.33$	
Density	$\rho = 2700$	kg/m ³

The LBIA, as shown in Figure 2, is equipped with integrated sensors that facilitate autonomous signal acquisition and output control. Moreover, the open-loop transfer function for LBIA with integrated piezoelectric sensors has been tested, as demonstrated in Figure 8.

From Figure 10a, it can be observed that the integrated design of LBIA proves effective in actively controlling the thin plate structure. The vibration energy in the first and second modes reduces by 8.1 dB and 7.3 dB, respectively. There is also some suppression in the fourth mode.

To provide a more accurate assessment of LBIA’s control performance, the control performances for LBIA using DVBF with different external sensors (such as a collocated accelerometer and non-collocated laser vibrometer) are also presented in this study. Figure 9b illustrates the placement of the accelerometer sensor on the sheet’s back, aligned with the

LBIA. Notably, the signal from the accelerometer sensor requires filtering through the signal conditioning instrument before being processed by the time integrator, which converts it into a velocity signal. This step completes the experimental setup for direct velocity feedback. Additionally, as shown in Figure 9c, the laser vibrometer's test point is located at the same position as the accelerometer sensor. The laser vibrometer directly collects the velocity signal of the vibration structure as the control signal, offering high acquisition accuracy without requiring any additional signal processing circuit. As a result, the LBIA's control effect on the structure can be more precisely evaluated.

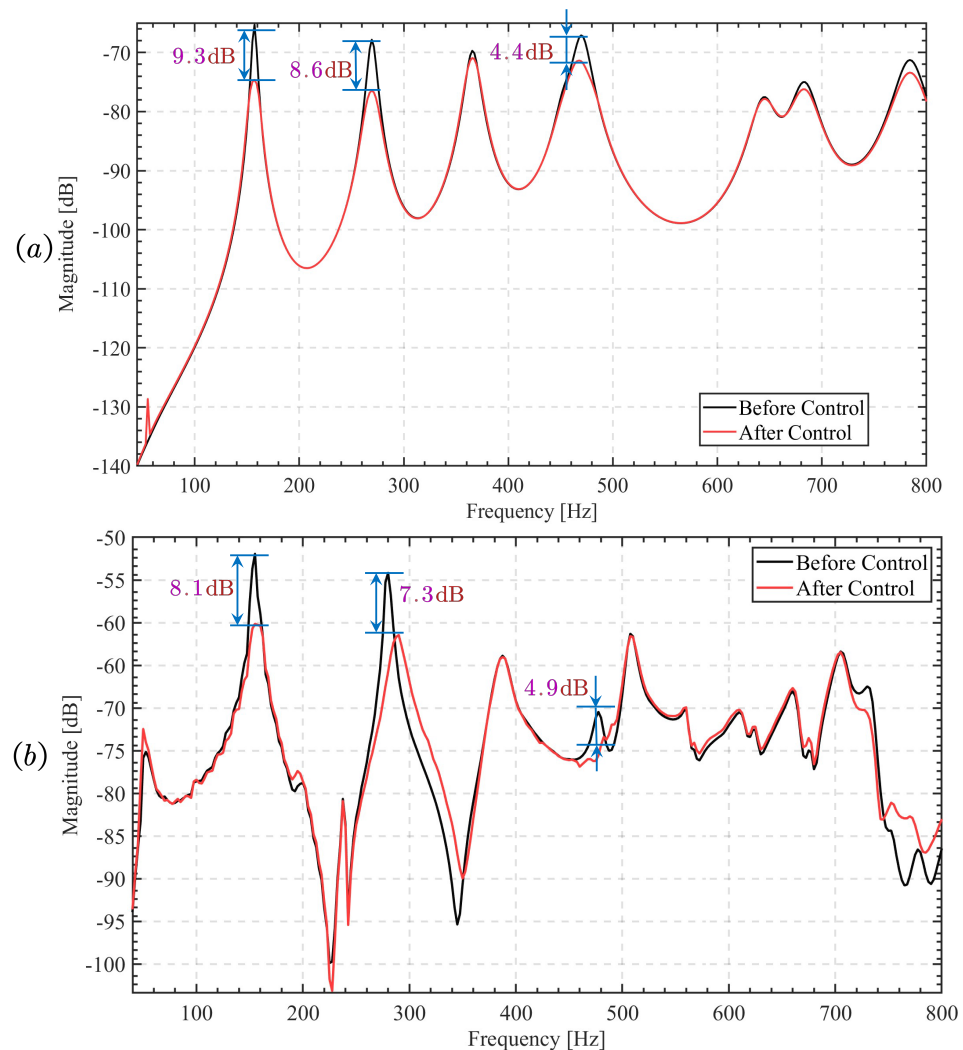


Figure 10. Control performance of LBIA with integrated sensor by using SDF approach: (a) calculation result; (b) experiment result.

Figure 11 demonstrates the control effect of the LBIA by illustrating the vibration energy of the system before and after implementing the control measures. Both the contact sensor and the non-contact sensor, utilizing negative velocity feedback, are employed in these measures. The LBIA significantly reduces vibration energy in the first and second modes, with reductions of 10.1 dB and 18.6 dB (contact sensor), and 12.3 dB and 23.6 dB (non-contact sensor), respectively. The use of high-precision non-contact sensors, such as a laser vibrometer, has demonstrated a positive control effect, which aligns with the numerical results. However, it is important to note that the integrated sensor design of the LBIA proves effective in active control but falls short in comparison to external sensors. The disparity arises mainly due to the piezoelectric ceramic sensor's sensitivity to the external environment, leading to interference signals that adversely affect control stability.

Despite this limitation, the low cost of the sensor (about USD 0.153) makes it a promising candidate for further research and suitable for large-scale vibration control in the industry. Consequently, the following section aims to enhance the control unit's effectiveness through multiple parallel bandpass filters.

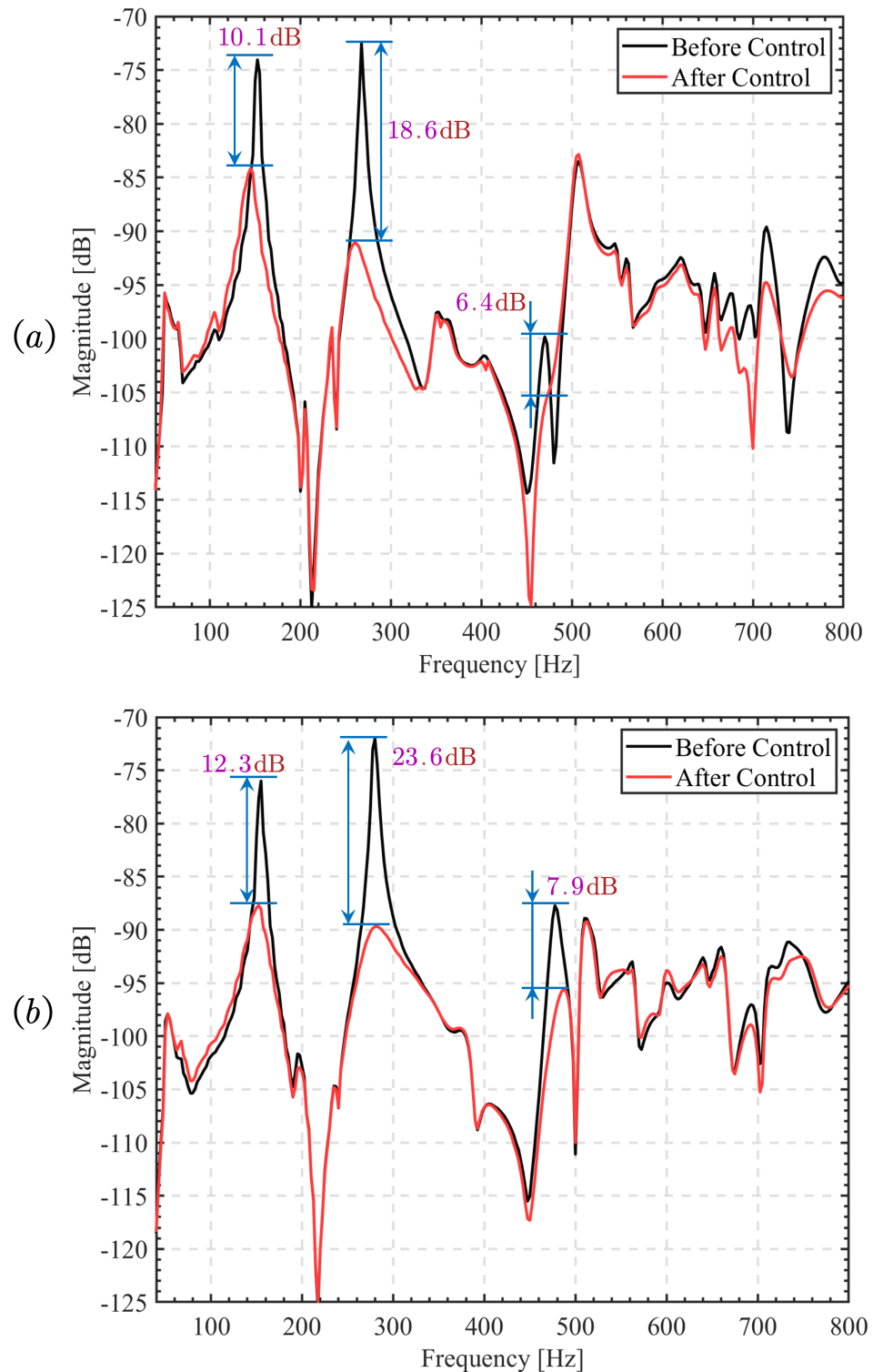


Figure 11. The effect diagram of control by DVBF: (a) accelerometer (contact sensor); (b) laser vibrometer (non-contact sensor).

4. Enhancing the Strain Differential Feedback Algorithm through Bandpass Filtering

4.1. Control Principle and Control Effect Simulation

To further improve the control performance of the proposed LBIA with an integrated piezoelectric sensor, the feedback control algorithm of the bandpass filter utilizes the strain differential signal (velocity signal) obtained from the LBIA with the integrated piezoelectric sensor as input. It enhances the damping of the controlled modes by employing multiple parallel bandpass filters, thereby facilitating active control of the multiple modes. Figure 12 depicts the control principal diagram of this algorithm.

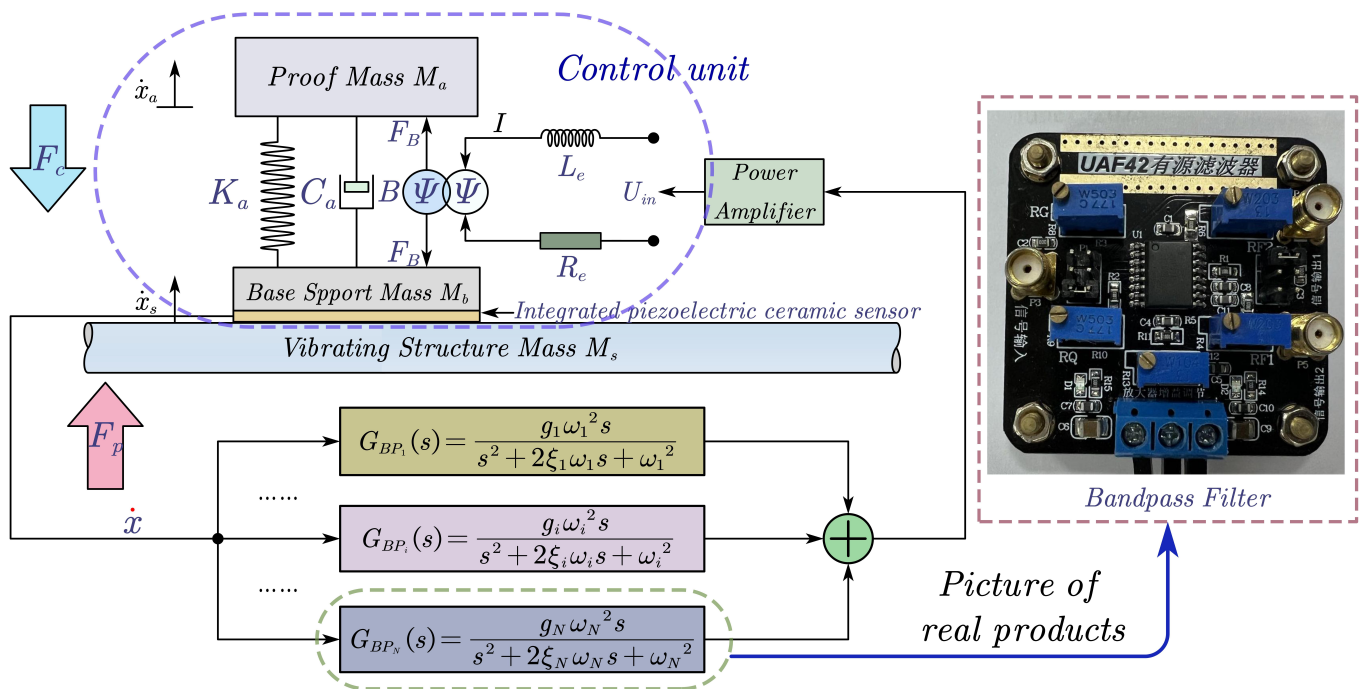


Figure 12. Schematic diagram of DVBF algorithm improved by bandpass filtering.

The LBIA employs an integrated piezoelectric ceramic sensor as the feedback mechanism. When the controlled structure is stimulated by F_p , the feedback sensor collects its vibration velocity signal. Subsequently, this signal is fed into an N-branch parallel bandpass filter, where it undergoes integration through an adder. Finally, the signal is sent to the LBIA via a power amplifier to generate the corresponding controlling force F_c , thus achieving closed-loop active control. Importantly, each bandpass filter’s natural frequency, damping ratio, and gain can be independently adjusted to suit specific requirements. The controller described is a parallel N-branch bandpass filter, and its output signal represents the summation of the basic velocity output from each branch bandpass filter, which can be expressed using the following Equation (16):

$$\begin{aligned}
 U_{in} &= Gain \cdot \sum_{i=1}^N G_{BP_i}(s) \dot{x} = Gain \cdot \dot{x} \sum_{i=1}^N \frac{g_i \omega_i s}{s^2 + 2\zeta_i \omega_i s + \omega_i^2} \\
 &= Gain \cdot \dot{x} \sum_{i=1}^N \frac{g_i \omega_i}{-\omega^2 + 2\zeta_i \omega_i s + \omega_i^2}
 \end{aligned}
 \tag{16}$$

where g_i , ζ_i , and ω_i represent the velocity feedback gain, damping ratio, and natural frequency of the nth branch bandpass filters, respectively. *Gain* refers to the amplification gain of a power amplifier.

According to Equations (1) and (2), we can derive the velocity transfer function of the inertial actuator after passing through N-branches:

$$T_{BP}(\omega) = \frac{\dot{x}_a}{\dot{x}_s} = \left[Gain \cdot \omega^2 \frac{Bl}{j\omega L_e + R_e} \cdot \sum_{i=1}^N \frac{g_i \omega_i}{\omega^2 - 2\zeta_i \omega_i s - \omega_i^2} + j\omega \left(\frac{(Bl)^2}{j\omega L_e + R_e} + C_a \right) + K_a \right] / \left[-\omega^2 M_a + j\omega \left(\frac{(Bl)^2}{j\omega L_e + R_e} + C_a \right) + K_a \right] \tag{17}$$

The velocity transfer in Equation (17) will be utilized to assess the multimodal control effect of the proposed controller combined with LBIA with integrated piezoelectric sensor, thereby providing theoretical calculation support for subsequent experiments.

4.2. Experiment Setup and Results

The primary objective of this experiment is to enhance the control effect of the LBIA with an integrated piezoelectric sensor by incorporating a low-cost, second-order bandpass filter, specifically designed using UAF42 (by Burr-Brown Inc., Tucson, AZ, USA). Figure 13 illustrates the schematic diagram of this specific bandpass filter.

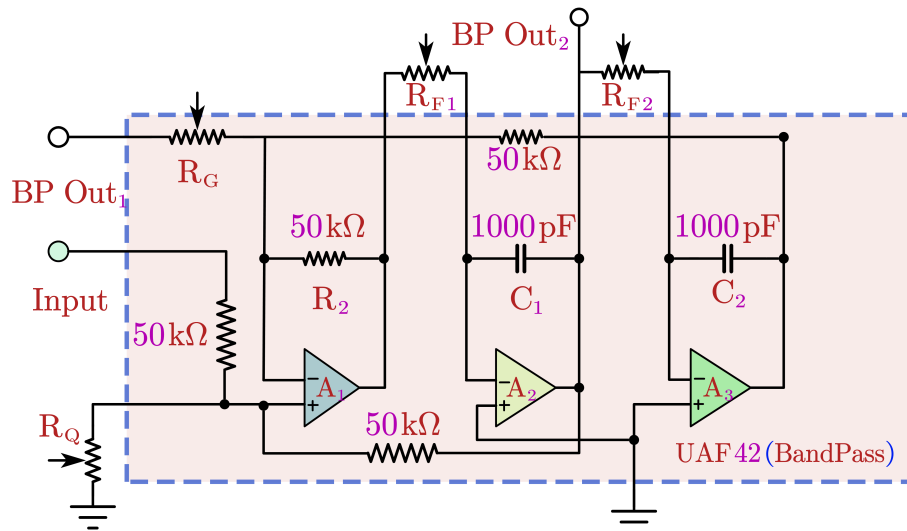


Figure 13. Diagram of a bandpass filter with reverse amplification function.

According to Figure 13, to facilitate the parameter adjustment in the experimental setup, R_G is set to a fixed value of 50 kΩ. The equation for adjusting the natural frequency, gain, and damping ratio of the bandpass filter designed based on UAF42 is derived as follows:

$$g_{BP} = \frac{25}{R_Q + 25} \tag{18}$$

$$\omega_n = \frac{10^9}{2\pi} \sqrt{\frac{1}{(R_{F1} \cdot R_{F2})}} \tag{19}$$

$$\zeta_n = \frac{1}{2 \cdot Q} = \sqrt{\frac{R_{F2}}{R_{F1}}} \cdot \frac{R_Q}{2R_Q + R_G} \tag{20}$$

where Q is the quality factor, which should be noted as inversely proportional to the passband gain. It is important to acknowledge that the Q value and the passband gain g_{BP} cannot be simultaneously maximized. When adjusting the setting, a certain balance must be achieved between the two.

After establishing the controller model, it is necessary to conduct further testing to evaluate the actual control effect of the LBIA with an integrated piezoelectric sensor combined with a bandpass filter. To accomplish this, the focus of the study is placed on a thin plate as the research object. A dedicated experimental platform is built, as illustrated in Figure 14. This experiment serves as an extension of the previous experiments. The position arrangement is the same as in the previous experiment but different control algorithms are used.

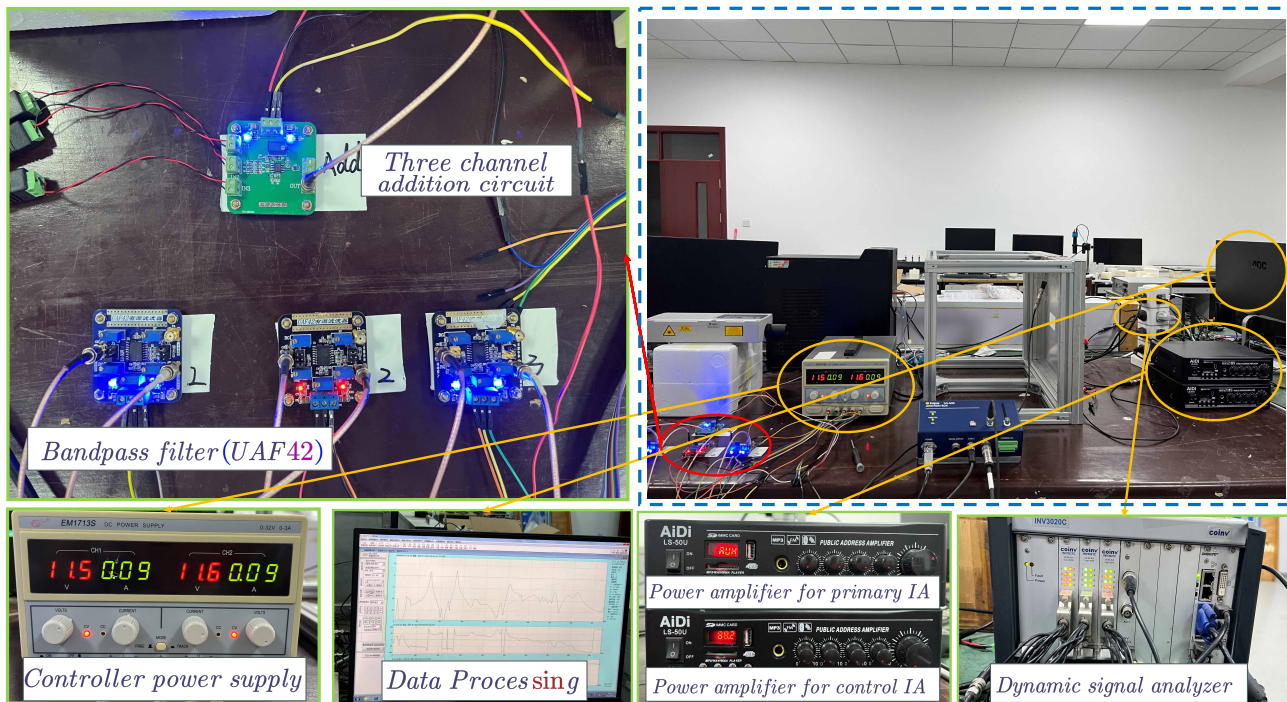


Figure 14. Experimental setup for bandpass filter velocity feedback control for a clamped–clamped thin plate using the LBIA.

To observe changes in the vibration energy of the controlled system, accelerometer sensors and a laser vibrometer are installed. Additionally, data acquisition and analysis software are configured for analyzing the experimental data. In this system, an integrated piezoelectric ceramic sensor is used to detect the vibration signal of the thin plate. The detected signal is then transmitted to three parallel bandpass filters. The output signals of these filters are combined using a three-way adder, and the resulting control signal is sent to the power amplifier to drive the inertial actuator for vibration suppression. This configuration forms a closed-loop control system.

Before conducting the experiment, it is essential to assess the characteristics of the multimodal controller based on multi-branch parallel features. This evaluation will pave the way for subsequent experiments. During the test, a sinusoidal signal sweeping from 0 to 800 Hz is passed through a dynamic analyzer equipped with three parallel bandpass filters.

Importantly, based on the theory and prior experiments mentioned above, the LBIA is capable of effectively controlling the first two and fourth modes from this control position. As a result, we can accurately predict the natural frequency of the bandpass filter using Equation (19). The calculated natural frequencies for the three bandpass filters are set to 156.25 Hz, 278.75 Hz, and 476.25 Hz, corresponding to the first two modes and the fourth mode of the thin plate structure. Additionally, the damping ratios for the filters are set to 0.12, 0.09, and 0.0625, respectively. Figure 15 shows the theoretical and experimental results of the velocity transfer functions of three parallel bandpass filters.

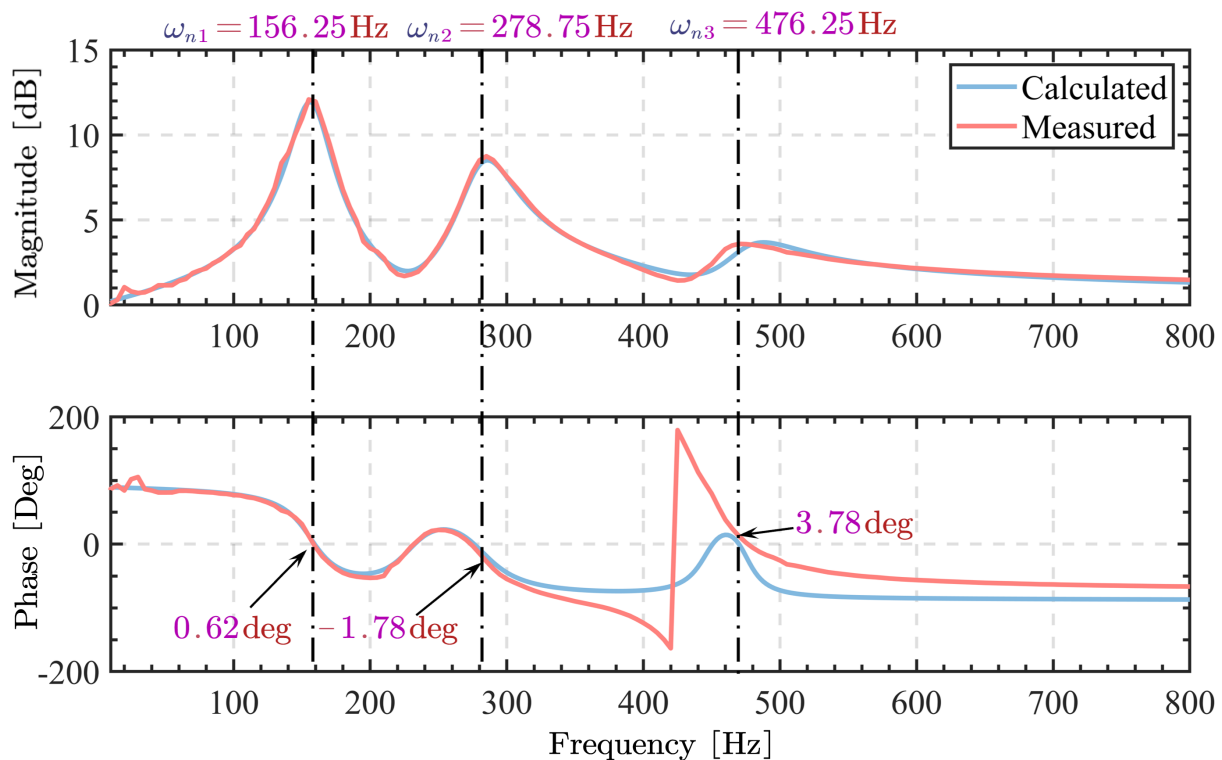


Figure 15. The velocity transfer function test diagram of bandpass filter is also combined.

According to Figure 15, the theoretical calculation of the bandpass filter is basically consistent with the experimental results. However, an interesting observation was made regarding a phase jump in the bandpass filter before reaching the third natural frequency of the control. Specifically, the phase first decays to -180 degrees and then rapidly jumps to approximately $+180$ degrees. This phase jump is a result of the relative positions of the poles and zeros of the filter. As the signal approaches the third-order operating frequency, the phase of the poles and zeros undergoes changes, leading to the occurrence of this phase jump. Additionally, at the operating frequency, the contributions of the poles and zeros to the phase cancel each other out, resulting in a phase of 0 degrees.

It is important to note that the phase jump is a normal phenomenon and does not adversely affect the performance of the filter. Despite the jump, the phase remains close to 0 degrees at the operating frequency and does not occur within the control frequency.

Figure 16 illustrates the calculated and experimental control performances of the LBIA with integrated piezoelectric sensor combined with three parallel bandpass filters. The experimental and calculation results demonstrate a high level of consistency. Notably, Figure 16b presents the control effect curve of the experimental test, revealing a reduction of approximately 10.6 dB in the peak value of the first mode and around 13.7 dB in the peak value of the second mode. Furthermore, the fourth mode is entirely suppressed. Intriguingly, the first and second modes exhibit the emergence of two new modes characterized by minimal damping. This damping effect primarily arises from the utilization of the bandpass filter, which efficiently absorbs vibration energy and enhances the control effect. The experimental curve aligns closely with the numerical calculation results, effectively introducing active damping for controlling structural vibration.

Nevertheless, disparities between the experimental and numerical approaches persist, attributable to several factors. Firstly, the measurement of structural vibration incurs inherent noise. Secondly, the experimental setup exhibits a resonance shift caused by non-ideal boundary conditions, in contrast to the simulations where full clamping is assumed. Finally, the imperfect match between the filter and sensor also impacts the performance of the control system.

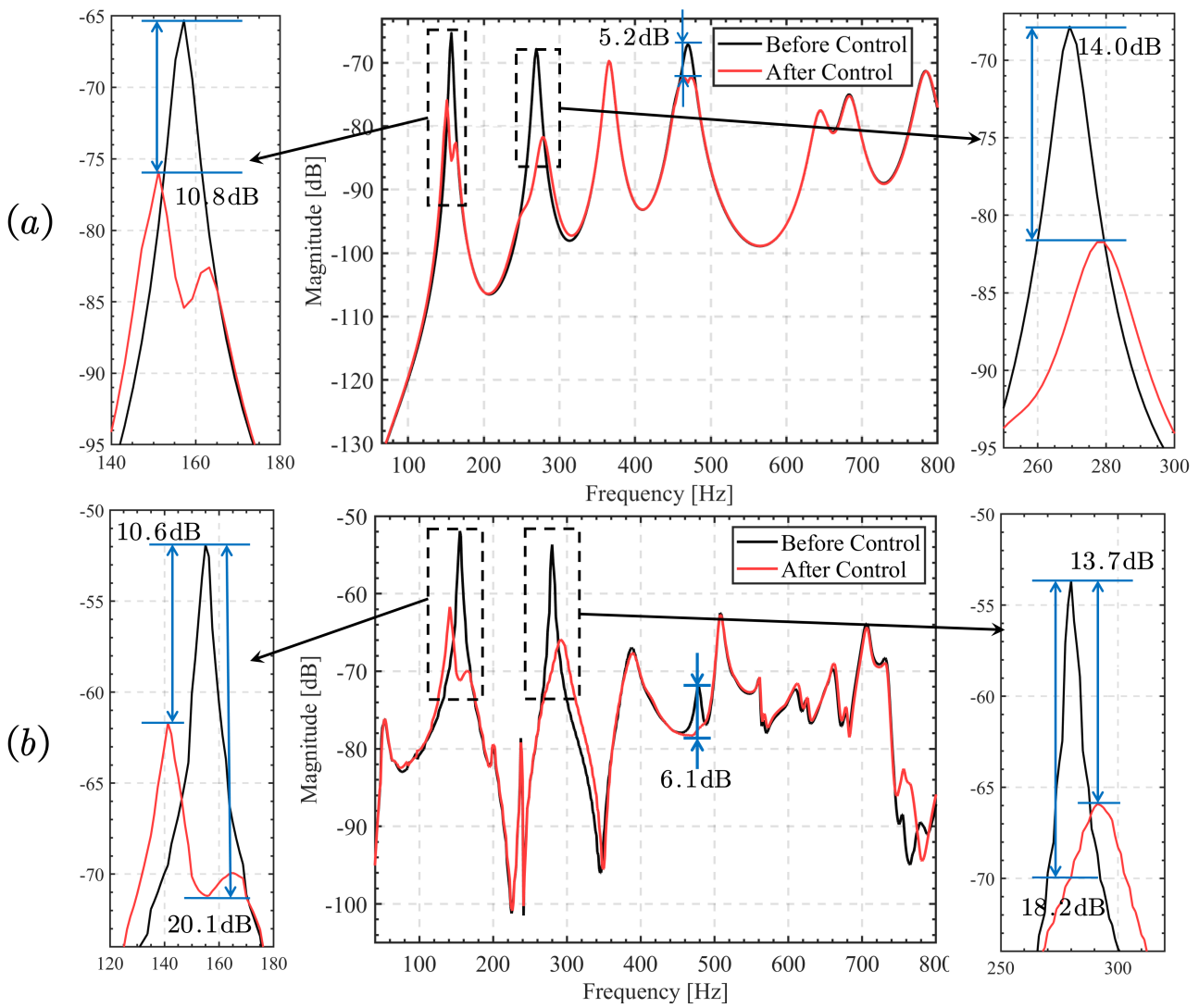


Figure 16. Bandpass filtering algorithm multimodal control effect. (a) Calculation result. (b) Experimental result.

Despite these variations, the model accurately captures the trends in the experimental results and serves as a suitable basis for comparison, thereby showcasing its efficacy.

Figure 17 displays time domain plots of acceleration before and after applying three different control solutions, all measured using the same positions of the velocity sensor and laser vibrometer. By examining the time domain diagram obtained from the velocity sensor, a comparison of the structural vibration state can be made between various control schemes under both uncontrolled and controlled conditions. Furthermore, Table 3 presents the percentage reduction in vibration for three control approaches.

Table 3. Comparison of FFT peak reduction rate with three control algorithms.

	Mode	Direct Velocity Feedback (Laser Vibrometer)	Strain Differential Feedback	Bandpass Filter
Reduction (%)	I	79.55%	49.53%	66.08%
	II	88.16%	77.55%	93.18%
	IV	61.05%	49.53%	66.08%

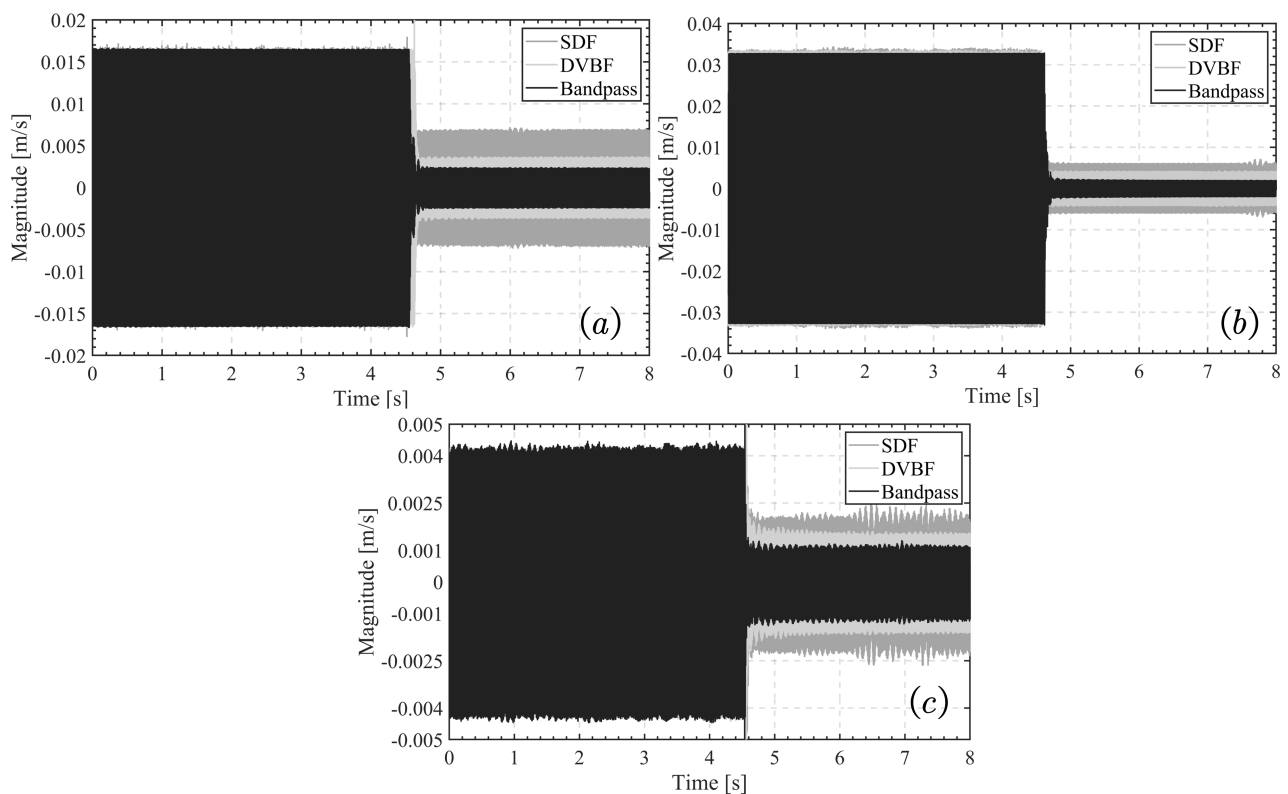


Figure 17. The experimental time domain results with different control approaches for (a) the first mode, (b) the second mode, and (c) the fourth mode.

From the observations of the percentage reduction, it can be concluded that mode II exhibits less damping than mode I, and mode I has less damping than mode IV. This pattern arises because, at this specific frequency, the inertial actuator efficiently transmits its force, leading to reduced vibration amplitudes. This mainly depends on the choice of control position and the design of the inertial actuator. Furthermore, the bandpass filter demonstrates the most effective control effect. It is capable of significantly reducing the vibration of the mode and further enhancing the control effect of the LBIA.

5. Discussion and Conclusions

This paper introduces an LBIA-integrated piezoelectric ceramic sensor control unit that serves as an inertial actuator for active vibration control. To achieve multimodal vibration control and enhance the control unit's effectiveness, a velocity feedback controller with multiple second-order bandpass filters in parallel is also used. The main findings of this study are outlined below:

Firstly, we completed the structural design of the LBIA as an inertial actuator and established its dynamic model and impedance model. The actuator's output characteristics and frequency response are tested on the experimental platform to verify the linear relationship between input and output, leading to the determination of the effective working frequency band.

Secondly, the integration of the piezoelectric ceramic sensor into LBIA as a separate control unit allows for establishing a mathematical model of the LBIA with piezoelectric ceramic sensor. The piezoelectric ceramic sensor converts its charge signal into a current signal through a current amplifier, resembling a differential process, which has been theoretically and experimentally proven. The resulting output current signal from the integrated sensor can be directly employed for actively controlling the vibrations of the structure. Additionally, the effectiveness of the control unit utilizing the SDF control

algorithm independently for vibration control of the thin plate structure is verified through numerical calculations and experiments.

Moreover, the effectiveness of LBIA for active control of thin plate structures is experimentally verified through its traditional direct velocity negative feedback algorithm. Experimental verification is conducted using the velocity sensor and acceleration sensor on the thin plate structure. The results demonstrate the homemade inertial actuator's effectiveness in controlling the first two modes of vibration of the thin plate structure and the fourth mode as well. The control effect is shown in Figure 10, with the observed reductions of 12.3 dB, 23.6 dB, and 7.9 dB being consistent with the numerical calculation results, thus confirming the superiority and reliability of the control design.

It is noteworthy that the integrated design of the control unit eliminates the need for additional cumbersome alignment operations to address the control problem. The sensors are adjusted to become velocity signals that are directly usable in the control loop, avoiding the need for additional external circuitry. Furthermore, the control unit adopts a lightweight design (32.4 g) with a low cost (about USD 2.5), enabling simple operation, cost-effectiveness, compact size, and effective control of the low-frequency-band mode of structural vibration.

Moreover, to enhance the control effect of the LBIA with an integrated piezoelectric ceramic thin plate, a well-designed bandpass filter velocity negative feedback control algorithm is developed. The main advantage of the bandpass filter lies in its ability to attenuate the vibration of multiple modes simultaneously. By setting the natural frequency of the bandpass filter equal to the control frequency of the target mode, the control effect of the target mode is significantly improved. Taking the thin plate structure as an example, the performance of the proposed bandpass filter's DVBF control is experimentally and numerically evaluated. The results show that, compared with the control unit, the control effect of the second mode is improved from 7.3 dB to 13.7 dB, with some improvement also observed in the first and second modes. The homemade inertial actuator effectively responds to the control signal processed by the filter and suppresses the vibration of the thin plate. The fourth-order natural frequency, as defined in this paper, may result from external noise; it can be conceptualized as a "non-resonant" frequency. Notably, it can be effectively regulated using a specifically designed bandpass filter to attenuate vibrations stemming from local responses. Consequently, this technique can be extended to address structural vibrations in diverse multiphysical environments, making it a promising direction for future research.

In summary, the LBIA with an integrated piezoelectric ceramic sensor, combined with the bandpass filter DVBF control algorithm proposed in this study, demonstrates remarkable results in multimodal vibration control. The lightweight design and low cost of the control unit provide valuable insights for its industrial application. Future research directions will include parameter optimization of the current method and its application to more complex structures, enabling wider applications of bandpass filters in multimodal control.

Author Contributions: M.C., original draft preparation, software, and experiment. Q.M., conceptualization, resources, project administration, funding acquisition, writing—review and editing, and supervision. L.P., data curation. Q.L., investigation. All authors have read and approved the final manuscript.

Funding: This work was sponsored by the National Natural Science Foundation of China (No. 12364058 and No. 51975266), the Aeronautical Science Foundation of China (No. 2020Z073056001), and the Graduate Innovative Special Fund Projects of Jiangxi Province (No. YC2023-S698).

Data Availability Statement: The data that support the findings of this study are available from the corresponding author upon reasonable request

Conflicts of Interest: The authors declare no conflict of interest.

References

1. Fuller, C.C.; Elliott, S.; Nelson, P.A. *Active Control of Vibration*; Academic Press: London, UK, 1996; pp. 1–2.
2. Hansen, C.; Snyder, S.; Qiu, X.; Brooks, L.; Moreau, D. *Active Control of Noise and Vibration*; CRC Press: Boca Raton, FL, USA, 2012; pp. 1–13.
3. Mao, Q.; Pietrzko, S. *Control of Noise and Structural Vibration*; Springer: London, UK, 2013; pp. 213–258.
4. Peláez-Rodríguez, C.; Magdaleno, A.; Iglesias-Pordomingo, Á.; Pérez-Aracil, J. Evolutionary Computation-Based Active Mass Damper Implementation for Vibration Mitigation in Slender Structures Using a Low-Cost Processor. *Actuators* **2023**, *12*, 254. [[CrossRef](#)]
5. Mao, Q.; Yuan, W.; Wu, J. Design and Experimental Study of a Multiple-Degree-of-Freedom Vibration Absorber by Using an Inertial Actuator. *Int. J. Struct. Stab. Dyn.* **2023**, *in press*. [[CrossRef](#)]
6. Elliott, S.J.; Rohlfing, J.; Gardonio, P. Multifunctional design of inertially-actuated velocity feedback controllers. *J. Acoust. Soc. Am.* **2012**, *131*, 1150–1157. [[CrossRef](#)]
7. Huyanan, S.; Sims, N.D. Vibration control strategies for proof-mass actuators. *J. Vib. Control* **2007**, *13*, 1785–1806. [[CrossRef](#)]
8. Mao, Q.; Li, S.; Huang, S. Inertial actuator with virtual mass for active vibration control. *Int. J. Acoust. Vib.* **2020**, *25*, 445–452. [[CrossRef](#)]
9. Díaz, I.M.; Reynolds, P. Robust saturated control of human-induced floor vibrations via a proof-mass actuator. *Smart Mater. Struct.* **2009**, *18*, 125024. [[CrossRef](#)]
10. Caresta, M.; Kessissoglou, N. Active control of sound radiated by a submarine hull in axisymmetric vibration using inertial actuators. *J. Vib. Acoust.* **2012**, *134*, 011002. [[CrossRef](#)]
11. Haase, T.; Unruh, O.; Algermissen, S.; Pohl, M. Active control of counter-rotating open rotor interior noise in a Dornier 728 experimental aircraft. *J. Sound Vib.* **2016**, *376*, 18–32. [[CrossRef](#)]
12. Díaz, C.G.; Gardonio, P. Feedback control laws for proof-mass electrodynamic actuators. *Smart Mater. Struct.* **2007**, *16*, 1766. [[CrossRef](#)]
13. Zilletti, M.; Elliott, S.J.; Gardonio, P. Self-tuning control systems of decentralised velocity feedback. *J. Sound Vib.* **2010**, *329*, 2738–2750. [[CrossRef](#)]
14. Rohlfing, J.; Gardonio, P.; Thompson, D.J. Comparison of decentralized velocity feedback control for thin homogeneous and stiff sandwich panels using electrodynamic proof-mass actuators. *J. Sound Vib.* **2011**, *330*, 843–867. [[CrossRef](#)]
15. Camperi, S.; Tehrani, M.G.; Elliott, S.J. Local tuning and power requirements of a multi-input multi-output decentralised velocity feedback with inertial actuators. *Mech. Syst. Signal Process.* **2019**, *117*, 689–708. [[CrossRef](#)]
16. Elliott, S.J.; Gardonio, P.; Sors, T.C.; Brennan, M.J. Active vibroacoustic control with multiple local feedback loops. *J. Acoust. Soc. Am.* **2002**, *111*, 908–915. [[CrossRef](#)] [[PubMed](#)]
17. Debattisti, N.; Bacci, M.L.; Cinquemani, S. Distributed wireless-based control strategy through Selective Negative Derivative Feedback algorithm. *Mech. Syst. Signal Process.* **2020**, *142*, 106742. [[CrossRef](#)]
18. Baudry, M.; Micheau, P.; Berry, A. Decentralized harmonic active vibration control of a flexible thin plate using piezoelectric actuator-sensor pairs. *J. Acoust. Soc. Am.* **2006**, *119*, 262–277. [[CrossRef](#)]
19. Balas, M. Feedback control of flexible systems. *IEEE Trans. Automat. Contr.* **1978**, *23*, 673–679. [[CrossRef](#)]
20. Gardonio, P.; Bianchi, E.; Elliott, S.J. Smart panel with multiple decentralized units for the control of sound transmission. Part I: Theoretical predictions. *J. Sound Vib.* **2004**, *274*, 163–192. [[CrossRef](#)]
21. Gardonio, P.; Bianchi, E.; Elliott, S.J. Smart panel with multiple decentralized units for the control of sound transmission. Part II: Design of the decentralized control units. *J. Sound Vib.* **2004**, *274*, 193–213. [[CrossRef](#)]
22. Gardonio, P.; Bianchi, E.; Elliott, S.J. Smart panel with multiple decentralized units for the control of sound transmission. Part III: Control system implementation. *J. Sound Vib.* **2004**, *274*, 215–232.
23. Silva, T.M.P.; Hameury, C.; Ferrari, G.; Balasubramanian, P.; Franchini, G.; Amabili, M. Particle swarm optimization of a non-collocated MIMO PPF active vibration control of a composite sandwich thin plate. *J. Sound Vib.* **2023**, *555*, 117723. [[CrossRef](#)]
24. Engels, W.P.; Baumann, O.N.; Elliott, S.J.; Fraanje, R. Centralized and decentralized control of structural vibration and sound radiation. *J. Acoust. Soc. Am.* **2006**, *119*, 025009. [[CrossRef](#)]
25. Camperi, S.; Tehrani, M.G.; Elliott, S.J. Parametric study on the optimal tuning of an inertial actuator for vibration control of a thin plate: Theory and experiments. *J. Sound Vib.* **2018**, *435*, 1–22. [[CrossRef](#)]
26. Zilletti, M.; Gardonio, P.; Elliott, S.J. Optimisation of a velocity feedback controller to minimise kinetic energy and maximise power dissipation. *J. Sound Vib.* **2014**, *333*, 4405–4414. [[CrossRef](#)]
27. Elliott, S.J.; Zilletti, M.; Gardonio, P. Self-tuning of local velocity feedback controllers to maximize power absorption. In *Recent Advances Structural Dynamics: Proceedings of the X International Conference, Southampton, UK, 12–14 July 2010*; Plymouth University: Plymouth, UK, 2010.
28. Gardonio, P.; Miani, S.; Blanchini, F.; Casagrande, D.; Elliott, S.J. Thin plate with decentralised velocity feedback loops: Power absorption and kinetic energy considerations. *J. Sound Vib.* **2012**, *331*, 1722–1741. [[CrossRef](#)]
29. Goh, C.J. Analysis and Control of Quasi-Distributed Parameter Systems. Ph.D. Dissertation, California Institute of Technology, Pasadena, CA, USA, 1983.
30. Fanson, J.L. An Experimental Investigation of Vibration Suppression in Large Space Structures Using Positive Position Feedback. Ph.D. Dissertation, California Institute of Technology, Pasadena, CA, USA, 1978.

31. Dosch, J.J.; Inman, D.J.; Garcia, E.A. A self-sensing piezoelectric actuator for collocated control. *J. Intell. Mater. Syst. Struct.* **1992**, *3*, 166–185. [[CrossRef](#)]
32. Dosch, J.J.; Leo, D.J.; Inman, D.J. Comparison of vibration control schemes for a smart antenna. In Proceedings of the 31st IEEE Conference on Decision and Control, Tucson, AZ, USA, 16–18 December 1992.
33. Jha, A.K.; Inman, D.J. Optimal sizes and placements of piezoelectric actuators and sensors for an inflated torus. *J. Intell. Mater. Syst. Struct.* **2003**, *14*, 563–576. [[CrossRef](#)]
34. El-Khoury, O.; Adeli, H. Recent advances on vibration control of structures under dynamic loading. *Arch. Comput. Methods Eng.* **2013**, *20*, 353–360. [[CrossRef](#)]
35. Fanson, J.L.; Caughey, T.K. Positive position feedback control for large space structures. *AIAA J.* **1990**, *28*, 717–724. [[CrossRef](#)]
36. Haase, F.; Kauba, M.; Mayer, D.; Van der Auweraer, H.; Gajdatsy, P.; de Oliveira, L.; da Silva, M.; Sas, P.; Deraemaeker, A. Active vibration control of an automotive firewall for interior noise reduction. In Proceedings of the Adaptronic Congress 2008, Berlin, Germany, 1 May 2008.
37. Omid, E.; Mahmoodi, N. Hybrid positive feedback control for active vibration attenuation of flexible structures. *IEEE/ASME Trans. Mechatron.* **2014**, *20*, 1790–1797. [[CrossRef](#)]
38. Preumont, A. *Vibration Control of Active Structures: An Introduction*; Springer: London, UK, 2018; pp. 47–66.
39. Friswell, M.I.; Inman, D.J. The relationship between positive position feedback and output feedback controllers. *Smart Mater. Struct.* **1999**, *8*, 285–291. [[CrossRef](#)]
40. Sim, E.; Lee, S.W. Active vibration control of flexible structures with acceleration feedback. *J. Guid. Control Dyn.* **1993**, *16*, 413–415. [[CrossRef](#)]
41. Zhao, G.; Paknejad, A.; Raze, G.; Deraemaeker, A.; Kerschen, G.; Collette, C. Nonlinear positive position feedback control for mitigation of nonlinear vibrations. *Mech. Syst. Signal Process.* **2019**, *132*, 457–470. [[CrossRef](#)]
42. Paknejad, A.; Zhao, G.; Osée, M.; Deraemaeker, A.; Robert, F.; Collette, C. A novel design of positive position feedback controller based on maximum damping and H2 optimization. *J. Vib. Control.* **2020**, *26*, 1155–1164. [[CrossRef](#)]
43. Balasubramanian, P.; Ferrari, G.; Hameury, C.; Silva, T.M.; Buabdulla, A.; Amabili, M. An experimental method to estimate the electro-mechanical coupling for active vibration control of a non-collocated free-edge sandwich thin plate. *Mech. Syst. Signal Process.* **2023**, *188*, 110043. [[CrossRef](#)]
44. Omid, E.; Mahmoodi, S.N.; Shepard, W.S., Jr. Multi positive feedback control method for active vibration suppression in flexible structures. *Mechatronics* **2016**, *33*, 23–33. [[CrossRef](#)]
45. Kournoutos, N.; Cheer, J. A system for controlling the directivity of sound radiated from a structure. *J. Acoust. Soc. Am.* **2020**, *147*, 231–241. [[CrossRef](#)]
46. Zhong, H.; Wu, J.; Bao, B.; Mao, Q. A composite beam integrating an in-situ FPCB sensor membrane with PVDF arrays for modal curvature measurement. *Measurement* **2020**, *166*, 108241. [[CrossRef](#)]
47. Mao, Q.; Zhong, H. Sound power estimation for beam and thin plate structures using polyvinylidene fluoride films as sensors. *Sensors* **2017**, *17*, 1111. [[CrossRef](#)]

Disclaimer/Publisher’s Note: The statements, opinions and data contained in all publications are solely those of the individual author(s) and contributor(s) and not of MDPI and/or the editor(s). MDPI and/or the editor(s) disclaim responsibility for any injury to people or property resulting from any ideas, methods, instructions or products referred to in the content.